Polymer 54 (2013) 1794–1802

Contents lists available at SciVerse ScienceDirect

Polymer

journal homepage: www.elsevier.com/locate/polymer

Synthesis of mesogen-jacketed liquid crystalline polymers with long symmetry mesogenic core containing two biphenyls

Sheng Chen, Hang Luo, He-Lou Xie, Hai-Liang Zhang*

Key Laboratory of Polymeric Materials and Application Technology of Hunan Province, Key Laboratory of Advanced Functional Polymer Materials of Colleges, and Universities of Hunan Province, College of Chemistry, Xiangtan University, Xiangtan 411105, Hunan Province, China

ARTICLE INFO

Article history:
Received 28 September 2012
Received in revised form
16 January 2013
Accepted 31 January 2013
Available online 8 February 2013

Keywords:
Liquid crystalline polymers
Phase behavior
Structure–property relation

ABSTRACT

A series of mesogen-jacketed liquid crystalline polymers, poly {2,5-bis[(4-alkoxybiphenyl)oxycarbonyl]-styrenes} (P-Cm, m = 8, 10, 12, 14 and 18) were designed and successfully synthesized via free radical polymerization. The chemical structures of the monomers were confirmed by ^{1}H NMR, ^{13}C NMR and Mass Spectrometry. The molecular characterizations of the polymers were performed with ^{1}H NMR, GPC and TGA. The phase structures and transitions of the polymers were investigated by the combination of techniques including DSC, POM, temperature-variable FT-IR spectroscopy, 1D WAXD and SAXS. The experimental results suggest that the polymers with symmetry mesogenic core containing two biphenyls can develop into a well-defined smectic A (S$_A$) phase. This implies that MJLCPs molecules shape can be modulated from rod-like to ribbon-like by simply changing the length of the mesogenic group.

1. Introduction

Liquid-crystalline polymers (LCPs) have attracted long standing attention for their potential applications in many fields, including optical data storage, optic, electro-optic, nonlinear optic devices, photomechanical and so on [1–7]. Generally speaking, LCPs have two main categories: main-chain liquid crystalline polymers (MCLCPs) with mesogen units located in the main chain [8–10] and side-chain liquid crystalline polymers (SCLCPs) with mesogens attached to the main chain as side groups [11,12]. For SCLCPs, Finkelmann pointed out that the flexible spacer inserted between main chain and mesogenic side groups was indispensable in order for a SC-LCP to achieve LC phase since it decoupled the interaction of side chain and polymer backbone, which disrupted the ordered packing of the side mesogens [13]. However, as proposed by Zhou et al., in 1987, mesogen jacketed liquid crystal polymers (MJLCPs), which were a special class of SCLCPs with their mesogenic units attached laterally to the main chain through a short spacer or with a single covalent bond, could also form stable LC phases [14–25]. Unlike the conventional SCLCPs whose backbones usually take a random-coil chain conformation, MJLCPs are somewhat rigid and exhibit some features of MCLCPs because the strong coupling between the polymer main chain and the highly crowded, rigid, and bulky side groups. So, the LC phase structures are found to be columnar nematic phase and hexagonal columnar phase in which each cylinder is formed by a single MJLCPs chain molecule.

However, the rod-like chain shall not be the only molecular shape of MJLCPs. Smectic phases have been found in laterally attached side-chain LC polymers by changing several variables, including the length or type of the terminal flexible substituent, chemical structures of mesogens, hydrogen bonding and the electrostatic interactions. For example, Padma Gopalan has reported the design, synthesis and characterization of MJLCPs with semi-fluorinated mesogenic groups (see Scheme 1(a)) [26]. Authors pointed out that the polymers could form S$_A$ phase because of the microphase separation. Through changing chemical structures of mesogens, Chen et al. have researched the phase behavior of MJLCPs with unbalanced mesogenic core and different terminal flexible substituents (see Scheme 1(b)) [27].The results showed that well-defined S$_A$ phase was formed when the carbon number for the flexible substituents were shorter than four (butoxy groups); whereas the one reached four, well-defined S$_C$ phase was observed. Chai et al. also have found that the MJLCPs containing the 1,3,4-oxadiazole unit exhibited S$_A$ phase (see Scheme 1(c)) [28]. Cheng et al. have found that the polymers contained amide linkages in the side groups formed S$_A$ phase due to hydrogen bonding (see Scheme 1(d)) [29]. Meantime, when the terminal groups were replaced by ionic groups, the polymers still presented S$_A$ phase because of the electrostatic interactions (see Scheme 1(e)) [30].

---

* Corresponding author. Tel.: +86 731 58293377; fax: +86 731 58293264.
E-mail addresses: hailiangzhang@xtu.edu.cn, zhanghangliang@xtu.edu.cn (H.-L. Zhang).

0032-3861/$ – see front matter © 2013 Elsevier Ltd. All rights reserved.
http://dx.doi.org/10.1016/j.polymer.2013.01.048

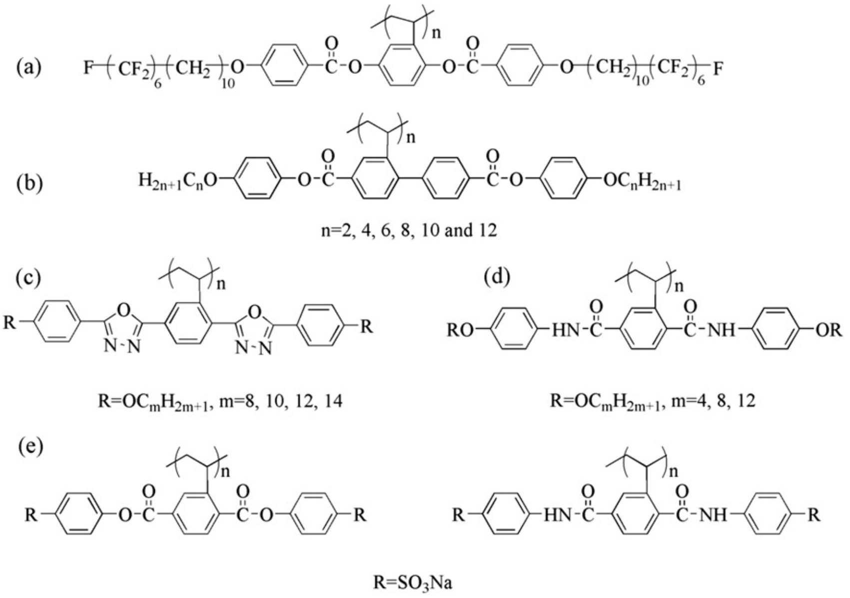

Scheme 1. Chemical structures of MJLCPs synthesized previously.

In our previous studies, we have systematically researched the influence of alkoxy tail length on the self-organization of poly {2,5-bis[(4-alkoxyphenyl)oxycarbonyl]styrenes} (P-OCm, m is the number of the carbons in the alkoxy groups, $m = 1, 2, 4, 6, 8, 10, 12, 14, 16$ and 18) based on 2-vinylterephthalic acid and 4-alkoxyphenyl (see Scheme 2(a)) [31].The experiments results demonstrated that the polymers could form smectic phase, isotropic phase and columnar phase when $m \geq 10$. The attachment of long flexible alkyl side chains to the polymer backbone can lead to layered structures due to the unfavorable interaction between mesogens and the apolar alkyl side chains, and it was considered that the smectic phase was proposed to form by the driving force of the enthalpy. Interesting point arises concerning the properties of MJLCPs when 4-alkoxyphenol was replaced by 4-alkoxybiphenol. One hand, compared with the rigid of core of the P-OCm, the new MJLCP (poly{2,5-bis[(4-alkoxybiphenyl) oxycarbonyl]styrene}, P-Cm) has a larger aspect ratio, leading to the stronger interaction between the side on rigid mesogens. The other hand, the phase behaviors of P-OCm were strongly alkyl length dependent due to the competing of the steric effect, the microphase separation and the driving force of the entropy. Of particular interest is to ask in whether the alkyl tails length has also influence on the phase behaviors of P-Cm. So, in this paper, we reported the synthesis and characterization of a series of vinyl monomers with different numbers of alkoxy terminal groups and their corresponding homopolymers. The chemical structures of polymers are shown in Scheme 2(b). However, the monomers M-Cm ($m < 8$) were found to be difficultly dissolved in common organic solvents or be polymerized to a sufficiently high Mn. Our experimental results proved that the polymers could develop into a stable S_A phase, whatever the alkyl tail length is short or long. Therefore, through studying the phase behavior of these polymers, we can deeply understand the relationship between a simple structural variable of the monomer and the change in the phase structure of MJLCPs.

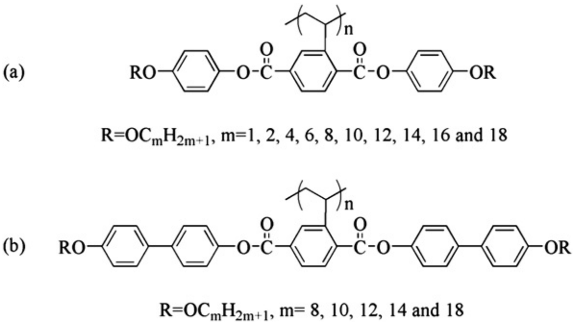

Scheme 2. Chemical structures of P-OCm (a) and P-Cm (b).

2. Experimental section

2.1. Materials

The precursor 2-vinylterephthalic acid (VTA) was synthesized according to previous paper [25]. Chlorobenzene (Acros, 99%) was purified by washing with concentrated sulfuric acid to remove residual thiophenes, followed by washing twice with distilled water, once with 5% sodium carbonate solution, and again with distilled water before being dried with anhydrous calcium chloride and then distilled. 4-(dimethylamino)pyridine (DMAP, 99%, ACROS), 4, 4′-Diphenol (98%, Alfa Aesar) and the corresponding octadecaoxyl bromides together with other reagents and solvents were used as received without further purification.

2.2. Synthesis of monomers

The synthetic route of monomers of 2,5-bis [(4-alkoxybiphenyl) oxycarbonyl]-styrenes (M-Cm, $m = 8, 10, 12, 14, 18$) is shown in Scheme 3. The experimental details are described as follows using 2,5-bis[(4-octanoxybiphenyl)oxycarbonyl]-styrene (M-C8) as an example.

2.2.1. Synthesis of 4-octanoxybiphenol

4, 4′-biphenol (20 g, 0.1074 mol), octyl bromide (3.5 g, 0.0182 mol), K_2CO_3 (14.964 g, 0.1086 mol) and 200 ml were added into a 500 ml round-bottom flask. The mixture was heated for 12 h in 55 °C, next the reaction mixture poured into a large amount of water to precipitate products. The products were purified by precipitation in water from THF solution three times. At last, the crude products were purified by column chromatograph (silica gel,

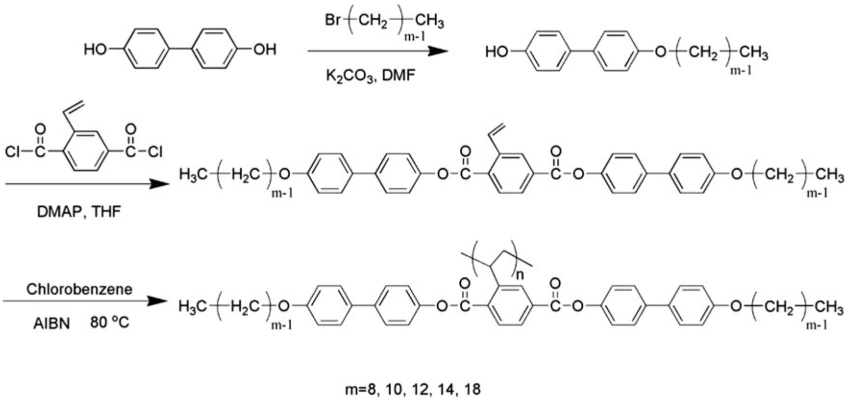

Scheme 3. Scheme of the synthesis of monomers and corresponding polymers.

CH_2Cl_2). The final product of 4-octanoxybiphenol was white powder with a yield of 3 g. ^{1}H NMR (400 HMz, $CDCl_3$): δ = 0.86–1.83 (m, 15, alkoxy H), 3.97–4.04 (t, 2H, $-OCH_2-$), 6.89–6.94 (m, 4H, Ar–*H*), 7.42–7.47(m, 4H, Ar–*H*).

2.2.2. *Synthesis of 5-bis[(4-octanoxybiphenyl)oxycarbonyl]-styrene (M-C8)*

VTA (5.2 mmol, 1 g) was added into 30 ml dried thionyl chloride in a 100 ml three-necked flask, then, the mixture was refluxed. After VTA was dissolved absolutely, the excess thionyl chloride was removed under reduced pressure. The residue was washed with petroleum ether for three times. The petroleum ether was removed under the reduced pressure and afforded yellow liquid. This liquid was dissolved in dried THF to obtain solution A. 4′-octanoxybiphenol (13.0 mmol, 3.86 g) and 4-(dimethylamino)pyridine (DMAP) (26.0 mmol, 3.18 g) were dissolved in 20 ml dried THF to obtain solution B. Under intense stirring at 0 °C, the solution A was slowly added into the solution B over a period of 2 h. The mixture was further stirred at room temperature for 12 h, and then most of the THF was distilled off by evaporation under reduced pressure. After water was added into the residue, the crude solid product was first collected by filtration and dried under vacuum, and then purified using column chromatography on silica gel with chloroform as eluant. ^{1}H NMR (400 HMz, $CDCl_3$): δ = 0.90–1.87 (m, 30H, alkoxy H), 4.01–4.04 (t, 4H, $-OCH_2-$), 5.52–5.91 (2d, 2H, $=CH_2$), 6.91–7.01 (m, 4H, Ar′–H–Ar), 7.28–7.33(m, 4H, 4H, Ar′–Ar–H), 7.53–7.55(4H, Ar′–H–Ar), 7.56–7.65 (m, 4H, Ar′–Ar–H and 1H, –CH=), 8.23–8.50 (m, 3H, Ar–H). ^{13}C NMR ($CDCl_3$): δ = 14.0.3 (–*CH*$_3$), 22.64 (–*CH*$_2$–), 26.09 (–*CH*$_2$–), 29.23–29.37 (–*CH*$_2$–), 31.82 (–*CH*$_2$–), 68.24 (–O*CH*$_2$–), 114.98 (=*CH*$_2$), 121.75 (aromatic *C* ortho to *C*–O), 127.81 (middle aromatic *C*), 128.13–128.72 (side aromatic *C*), 129.18 (middle aromatic *C*), 131.00 (middle aromatic *C*), 132.12–132.67 (side aromatic *C*), 133.29 (middle aromatic *C*), 134.71 (–*HC*=*CH*$_2$), 139.12 (aromatic *C*–HC=CH$_2$), 149.66–149.77 (side aromatic *C*–O), 158.98 (side aromatic *C*–O), 164.33–165.11 (*C*=O). Mass Spectrometry (MS) (*m*/*z*) [M] Calcd for $C_{50}H_{56}O_6$, 752.41; found, 751.228 + 1.

2.2.3. *Synthesis of 2,5-bis [(4-alkoxybiphenyl)oxycarbonyl]-styrenes (M-Cm, m = 10, 12, 14, 18)*

All the other monomers were synthesized and characterized similarly. The characterization data of M-Cm (*m* = 10, 12, 14 and 18) were as follows:

2.2.3.1. 2,5-bis[(4-decyloxybiphenyl)oxycarbonyl]styrene (M-C10). ^{1}H NMR (400 HMz, $CDCl_3$): δ = 0.87–1.87 (m, 38H, alkoxy H), 4.01–4.04 (t, 4H, $-OCH_2-$), 5.52–5.91 (2d, 2H, $=CH_2$), 6.99–7.01 (m, 4H, Ar′–H–Ar), 7.28–7.33(m, 4H, 4H, Ar′–Ar–H), 7.53–7.55(4H, Ar′–H–Ar), 7.56–7.65 (m, 4H, Ar′–Ar–H and 1H, –CH=), 8.25–8.51 (m, 3H, Ar–H). ^{13}C NMR ($CDCl_3$): δ = 14.10 (–*CH*$_3$), 22.70 (–*CH*$_2$–), 26.12 (–*CH*$_2$–), 29.37–29.62 (–*CH*$_2$–), 31.94 (–*CH*$_2$–), 68.24 (–O*CH*$_2$–), 114.99 (=*CH*$_2$), 121.78 (aromatic *C* ortho to *C*–O), 127.8 (middle aromatic *C*), 128.14–128.74 (side aromatic *C*), 129.17 (middle aromatic *C*), 131.03 (middle aromatic *C*), 132.08–132.65 (side aromatic *C*), 133.30 (middle aromatic *C*), 134.73 (–*HC*=*CH*$_2$), 139.14 (aromatic *C*–HC=CH$_2$), 149.66–149.77 (side aromatic *C*–O), 159.00 (side aromatic *C*–O), 164.30–165.08 (*C*=O). Mass Spectrometry (MS) (*m*/*z*) [M] Calcd for $C_{54}H_{64}O_6$, 808.47; found, 807.544 + 1.

2.2.3.2. 2,5-bis[(4-dodecyloxybiphenyl)oxycarbonyl]styrene (M-C12). ^{1}H NMR (400 HMz, $CDCl_3$): δ = 0.89–1.87 (m, 46H, alkoxy H), 4.01–4.04 (t, 4H, $-OCH_2-$), 5.52–5.91 (2d, 2H, $=CH_2$), 6.99–7.02 (m, 4H, Ar′–H–Ar), 7.28–7.33(m, 4H, 4H, Ar′–Ar–H), 7.53–7.55(4H, Ar′–H–Ar), 7.56–7.65 (m, 4H, Ar′–Ar–H and 1H, –CH=), 8.23–8.50 (m, 3H, Ar–H). ^{13}C NMR ($CDCl_3$): δ = 14.12 (–*CH*$_3$), 22.73 (–*CH*$_2$–), 26.14 (–*CH*$_2$–), 29.40–29.67 (–*CH*$_2$–), 31.98 (–*CH*$_2$–), 68.25 (–O*CH*$_2$–), 115.02 (=*CH*$_2$), 121.79 (aromatic *C* ortho to *C*–O), 127.78 (middle aromatic *C*), 128.13–128.73 (side aromatic *C*), 129.17 (middle aromatic *C*), 131.04 (middle aromatic *C*), 132.12–132.66 (side aromatic *C*), 133.32 (middle aromatic *C*), 134.72 (–*HC*=*CH*$_2$), 139.12 (aromatic *C*–HC=CH$_2$), 149.70–149.81 (side aromatic *C*–O), 159.03 (side aromatic *C*–O), 164.26–165.06 (*C*=O). Mass Spectrometry (MS) (*m*/*z*) [M] Calcd for $C_{58}H_{72}O_6$, 864.53; found, 863.315 + 1.

2.2.3.3. 2,5-bis[(4-tetradecyloxybiphenyl)oxycarbonyl]styrene (M-C14). ^{1}H NMR (400 HMz, $CDCl_3$): δ = 0.88–1.87 (m, 54H, alkoxy H), 4.01–4.04 (t, 4H, $-OCH_2-$), 5.52–5.91 (2d, 2H, $=CH_2$), 6.99–7.01 (m, 4H, Ar′–H–Ar), 7.28–7.33(m, 4H, 4H, Ar′–Ar–H), 7.53–7.55(4H, Ar′–H–Ar), 7.56–7.65 (m, 4H, Ar′–Ar–H and 1H, –CH=), 8.23–8.50 (m, 3H, Ar–H). ^{13}C NMR ($CDCl_3$): δ = 14.07 (–*CH*$_3$), 22.67 (–*CH*$_2$–), 26.15 (–*CH*$_2$–), 29.35–29.60 (–*CH*$_2$–), 31.92 (–*CH*$_2$–), 68.23 (–O*CH*$_2$–), 114.95 (=*CH*$_2$), 121.75 (aromatic *C* ortho to *C*–O), 127.74 (middle aromatic *C*), 128.10–128.71 (side aromatic *C*), 129.14 (middle aromatic *C*), 131.01 (middle aromatic *C*), 132.14–132.62 (side aromatic *C*), 133.31 (middle aromatic *C*), 134.71 (–*HC*=*CH*$_2$), 139.08 (aromatic *C*–HC=CH$_2$), 149.70–149.79 (side aromatic *C*–O), 159.11 (side aromatic *C*–O), 164.25–165.04 (*C*=O). Mass Spectrometry (MS) (*m*/*z*) [M] Calcd for $C_{62}H_{80}O_6$, 920.6; found, 919.431 + 1.

2.2.3.4. 2,5-bis[(4-octadecaoxybiphenyl)oxycarbonyl]-styrene (M-C18). ^{1}H NMR (400 HMz, $CDCl_3$): δ = 0.86–1.84 (m, 70H, alkoxy H), 3.96–4.02 (t, 4H, $-OCH_2-$), 5.51–5.90 (2d, 2H, $=CH_2$), 6.91–7.00 (m, 4H, Ar–Ar′–H), 7.28–7.33(m, 4H, Ar–H–Ar′), 7.51–7.65 (m, 4H, Ar–Ar′–H and m, 4H, Ar–H–Ar′ and 1H, –CH=), 8.23–8.50 (m, 3H, Ar–H). ^{13}C NMR (CDCl$_3$): δ = 14.06 (–CH_3), 22.67 (–CH_2–), 26.09(–CH_2–), 29.35–29.70 (–CH_2–), 31.93 (–CH_2–), 68.24 (–OCH_2–), 114.99 (=CH_2), 121.75 (aromatic *C* ortho to *C*–O), 127.65 (middle aromatic *C*), 128.13–128.75 (side aromatic *C*), 129.15 (middle aromatic *C*), 131.04 (middle aromatic *C*), 132.15–132.67 (side aromatic *C*), 133.34 (middle aromatic *C*), 134.75 (–*HC*=CH_2), 139.15 (aromatic *C*–HC=CH_2), 149.64–149.72 (side aromatic *C*–O), 159.11 (side aromatic *C*–O), 164.28–165.04 (*C*=O). Mass Spectrometry (MS) (*m*/*z*) [M] Calcd for $C_{70}H_{96}O_6$, 1032.72; found, 1031.571 + 1.

2.3. Polymerization

All the polymers were synthesized by conventional solution radical polymerization (see Scheme 3). For example, 0.752 g (1 mmol) of M-C8, 100 μL of chlorobenzene solution of 0.01 mmol AIBN, 2 ml of chlorobenzene and a magnetic stir bar were added into a polymerization tube, the tube was purged with nitrogen and subjected to four freeze–thaw cycles to remove any dissolved oxygen and sealed off under vacuum. Polymerization was carried out at 80 °C for 24 h. The tube was then opened, and the reaction mixture was diluted with 20 ml THF. The resultant polymer was precipitated and washed with acetone. To eliminate the unreacted monomers completely, the purification was repeated, until no peak was observed at the elution time of monomer in gel permeation chromatography (GPC) measurement.

2.4. Instruments and measurements

^{1}NMR measurements were performed on a Bruker ARX400 MHz spectrometer using with CDCl$_3$ as solvent, tetramethylsilane (TMS) as the internal standard at room temperature.

The apparent number-average molecular weight (M_n) and polydispersity index (PDI = M_w/M_n) were measured on a GPC (WATERS 1515) instrument with a set of HT3, HT4 and HT5. The μ-styragel columns used THF as an eluent and the flow rate was 1.0 ml/min at 38 °C. All the GPC data were calibrated with polystyrene standards.

TGA was performed on a TA-SDT 2960 instrument at a heating rate of 20 °C/min in nitrogen atmosphere.

DSC traces of all the polymers were obtained using a TA-Q10 DSC instrument. The temperature and heat flow were calibrated using standard materials (indium and zinc) at a cooling and heating rates of 10 °C/min. Samples with a typical mass of about 5 mg were encapsulated in sealed aluminum pans.

FTIR spectra in KBr pellets were recorded on a PE Spectrum One FTIR spectrophotometer.

LC texture of the polymers was examined under POM (Leica DM-LM-P) equipped with a Mettler-Toledo hot stage (FP82HT).

One-dimensional (1D) wide-angle X-ray diffraction (WAXD) experiments were performed on a Philips X'Pert Pro diffractometer with a 3 kW ceramic tube as the X-ray source (Cu Kα) and an X'celerator detector. The sample stage was set horizontally. The reflection peak positions were calibrated with silicon powder ($2\theta > 15°$) and silver behenate ($2\theta < 10°$). A temperature control unit (Paar Physica TCU 100) in conjunction with the diffractometer was utilized to study the structure evolutions as a function of temperature.

Small-angle X-ray scattering (SAXS) experiments were performed using a high-flux SAXS instrument (SAXSess, Anton Paar) equipped with Kratky block-collimation system and a Philips PW3830 sealed-tube X-ray generator (Cu KR). The wavelength was 0.1542 nm. A highly sensitive SAXS imaging plate which was 264.5 mm away from the sample was used to collect the signal in

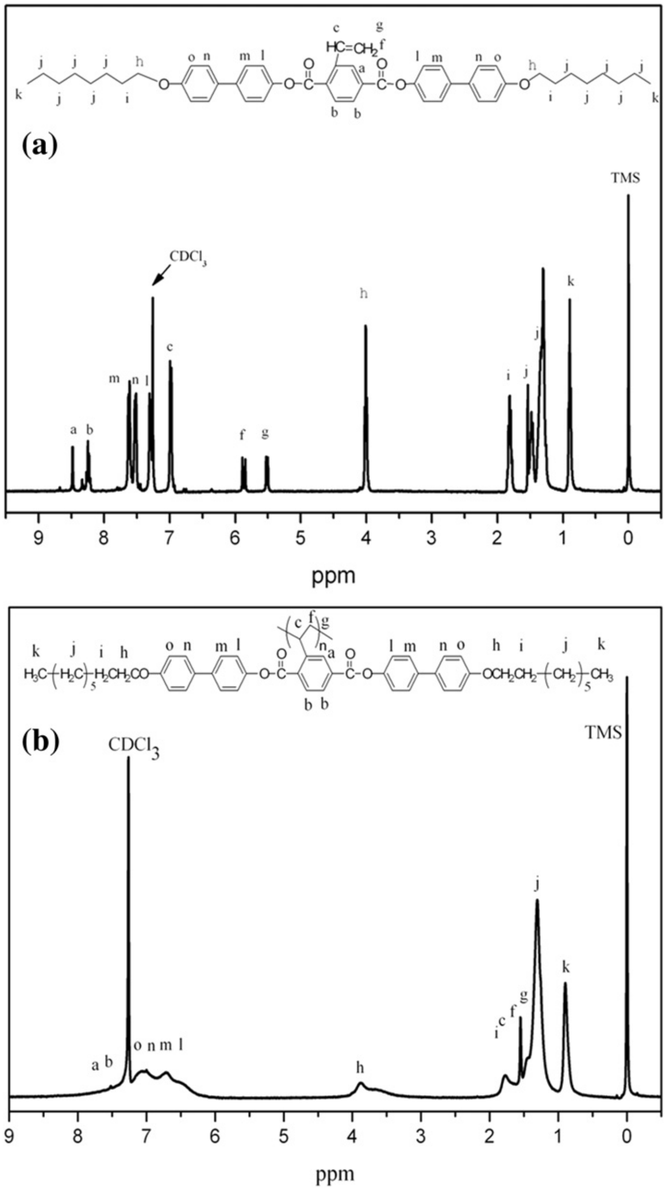

Fig. 1. ^{1}H NMR spectrums of the monomer M-C8 (a) and the polymer P-C8 (b) in CDCl$_3$.

Table 1
Molecular characteristics of polymers.

Sample	$M_n(\times 10^5)$[a]	PDI[a]	Tm[b]	Tg[b]	Td[c]	Liquid crystallinity[d]
P-C8	2.47	2.4	–	225.9	424	Yes
P-C10	1.75	2.2	–	222.6	424	Yes
P-C12	1.52	2.5	−4.8	221.3	426	Yes
P-C14	1.60	2.2	23.2	211.9	421	Yes
P-C18	1.87	2.0	52.7	192.4	414	Yes

[a] Relative M_n and polydispersity (PDI) were measured by GPC using PS standards.

[b] The melting temperatures and the glass transition temperatures were measured by DSC at a heating rate of 10 °C/min under nitrogen atmosphere during the second heating process.

[c] The temperatures at 5% weight loss of the samples under nitrogen [Td(N_2)] were measured by TGA heating experiments at a rate of 20 °C/min.

[d] The liquid crystallinity was observed by POM.

Table 2
Liquid crystallinities of the monomers.

Monomers	Phase transitions (°C)	
	First cooling	Second heating
M-C8	N 97.2 S 87.6 Cr 2.4	Cr 98.6 S 118.09 N
M-C10	N 96.57 S 89.4 Cr 2.2	Cr$_1$ 105.6 Cr$_2$ 110.5 S 124.9 N
M-C12	N 95.4 Cr	Cr$_1$ 109.7 Cr$_2$ 125.2 N
M-C14	N 98.3 Cr	Cr$_1$ 114.1 Cr$_2$ 120.8 N
M-C18	N 95.1 Cr	Cr 111.1 N

Cr: crystalline; N: nematic; and S: smectic phase.

vacuum. Samples were placed in between aluminum foils which were folded and sandwiched in a steel sample holder. After background subtraction, desmearing was performed according to the Lake's method. A temperature control unit (Anton Paar TCS300) in conjunction with the SAXSess was utilized to study the structure at various temperatures.

3. Results and discussion

3.1. Synthesis and characterization of monomers and polymers

All the monomers could be easily polymerized via free radical polymerization. Herein, we use P-8C as an example to elucidate the process. Part (a) and (b) of Fig. 1 give the ^{1}H NMR spectra ($CDCl_3^{-d}$) of the monomer M-C8 and the polymer P–C8, respectively. The M-C8 showed the characteristic resonances of the vinyl group at 5.52–5.91 and 7.51–7.60 ppm. After polymerization, these signals disappeared completely. The chemical shifts of P–C8 were quite broad and consistent with the expected polymer structure. In order to remove the influence of M_n on the LC behaviors, we synthesized a series of polymers with the similar M_n. The molecular characterizations of the polymers are summarized Table 1. At the same time, the apparent number-average molecular weights (M_n's) of the polymers determined by GPC were higher than 1.5×10^5 g/mol, demonstrating good polymerizability of the monomers.

3.2. Mesomorphic properties of the monomers

The phase behaviors of the monomers M-Cm ($m = 8, 10, 12, 14$ and 18) were examined by the conventional analyses including DSC and POM. In order to avoid the thermal polymerization, the detection temperature of DSC and POM was below 200 °C. The thermograms of M-Cm on both first cooling scans and the second heating are illustrated in supporting information Fig. S1, and their phase transition temperatures are collected in Table 2. The results showed that all the monomers presented crystal phase in low temperature (Fig. 2(a)) and formed nematic phase in high temperature (Fig. 2(c)). Moreover, nematic phase didn't disappear above 200 °C under POM. In addition, in the intermediate temperature, the M-C8 and M-C10 exhibited smectic phase (Fig. 2(b)).

3.3. Phase transitions and phase structures of the polymers

Fig. 3 shows that all polymers have good thermal stability, i.e., the temperatures at 5% weight loss of the samples under nitrogen were about 410 °C measured by TGA at a rate of 20 °C/min (see Table 1), indicating the strong interaction among the biphenyl moieties. Fig. 4 shows the second heating DSC curves of P-Cm ($m = 8$, 10, 12, 14 and 18) at a rate of 10 °C/min under nitrogen atmosphere after eliminating the thermal history. As can be seen, the glass transitions (Tg) of all polymers can be observed, and were basically decreased with the increasing of the length of alkyl because of the intrinsic plastification of the alkoxy tails (listed in

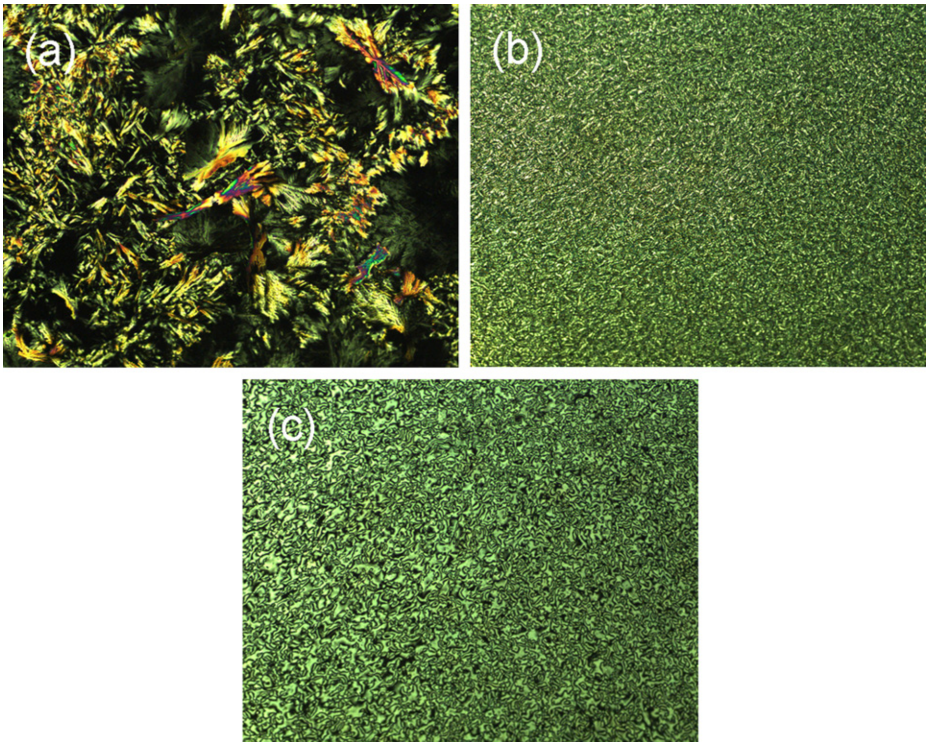

Fig. 2. Representative POM images of the texture of M-C8 at (a) 80 °C, (b) 95 °C and (c) 140 °C (magnification: ×200).

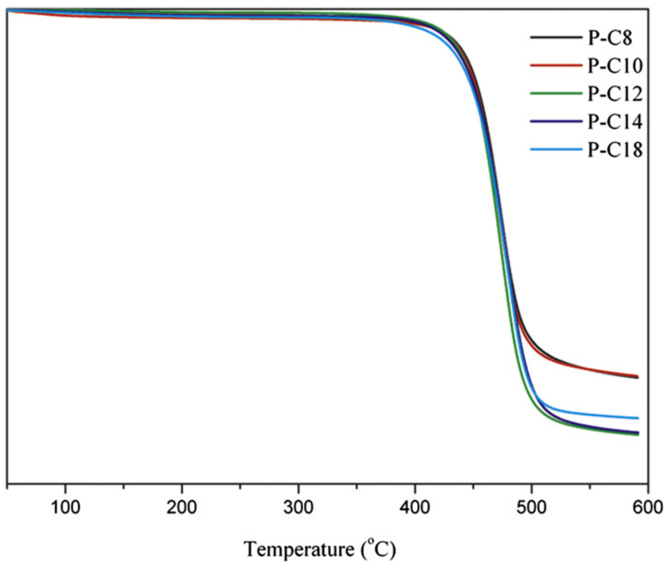

Fig. 3. TGA diagrams of polymers in N_2 at a rate of 20 °C/min.

Table 1). Contrast to the Tg of P-OCm, the Tg of P-Cm is much higher because of the bulkier structure of mesogens. It also indicates that side chains have the strong interaction, hindering the movement of main chains. Beside Tg, the melting points of the alkoxy tails can be seen for P-C12, P-C14 and P-C18. After Tg, no more transition peaks were seen. The phenomenon is similar to some other MJLCPs systems [27].

In order to further elucidate the phase transition and macromolecular chain mobility in the polymers, VT-FTIR experiments were carried out. It is well known the rocking vibration at ca. 720 cm^{-1} and scissoring vibration at ca. 1470 cm^{-1} are taken into account as the characteristic bands of methylene group, which are sensitive to the conformational variation as well as the environmental alternation [32]. The rocking vibrational FTIR spectra of the P-C18 are shown in Fig. 5 (a). In heating process, the intensity of rocking band at 720 cm^{-1} decreased with temperature increasing. Moreover, the sudden changed emerges at 40–75 °C, which is consistent with DSC results, indicating that crystalline structure of alkoxy side chain was transformed to disordered state. Fig. 5 (b) shows the VT-FTIR spectra of P–C18 in the range of 1490–1450 cm^{-1}. The peaks around 1466 cm^{-1} and 1457 cm^{-1} correspond to the trans and gauche conformational structure of methylene group (CH_2), respectively [32]. It can be seen that the intensity of trans conformational band at 1466 cm^{-1} decreases with increasing temperature, while the intensity of gauche conformational band at 1457 cm^{-1} increases. Therefore we can make a conclusion that the conformation of alkoxy side chain in P-C18 experiences a variation process from stable structure (trans) to metastable structure (gauche) during the heating process.

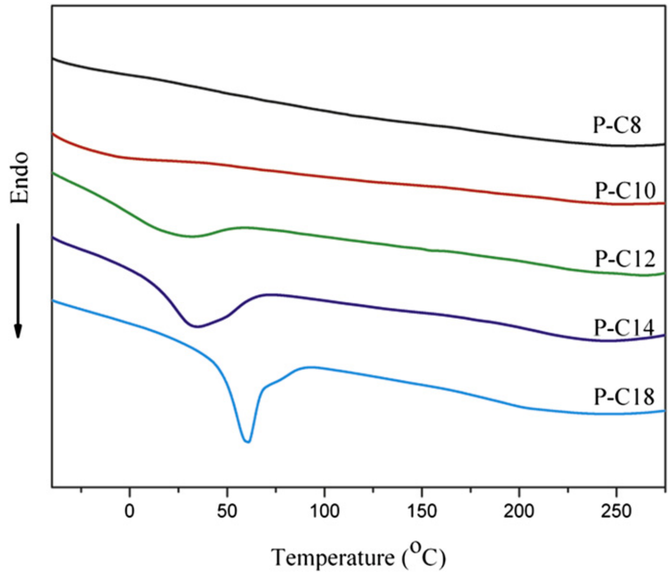

Fig. 4. DSC curves of P-Cm during the second heating scan at a rate of 10 °C/min under nitrogen atmosphere.

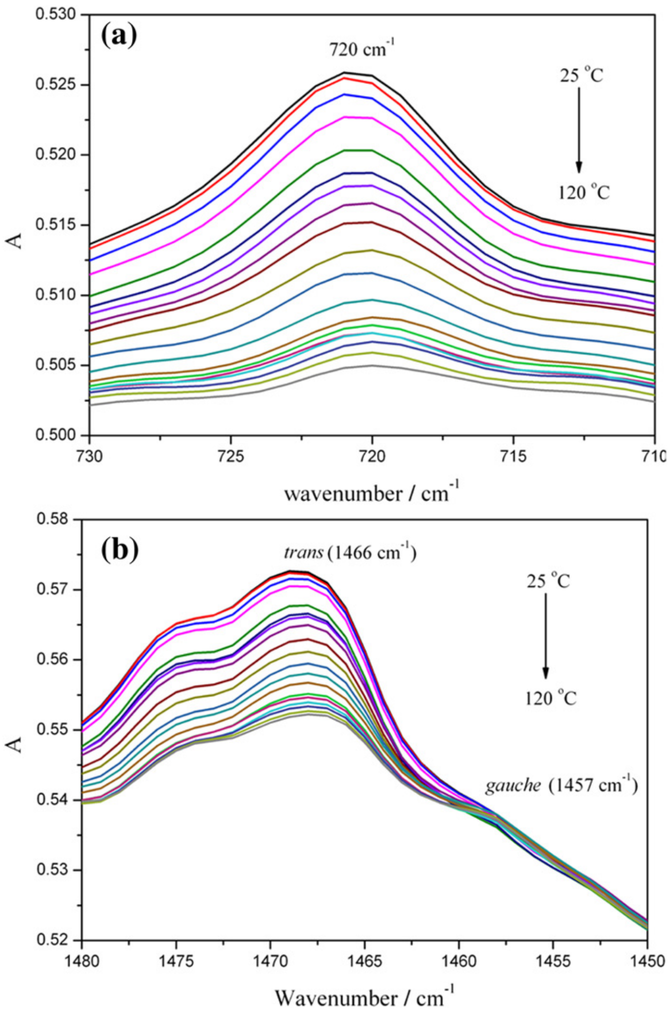

Fig. 5. Temperature-variable FT-IR spectra of (a) methylene rocking band for the sample P-C18 and (b) methylene scissoring band for the sample P-C18. Heating process, from top to bottom: 25, 30, 35, 40, 45, 50, 55, 60, 65, 70, 75, 80, 85, 90, 95, 100, 105, 110 and 120 °C.

Birefringence of the polymers is observed by POM. All samples were cast from THF solution and slowly dried at room temperature, then slowly heated. The POM images of polymers were shown in Fig. 6 when heating to 150 °C, showing that all polymers formed the LC phase. Especially, for P-C18, the needle-like texture was observed, indicating the polymer formed smectic phase. For this, it may be that the polymers with longer alkyl group had the lower Tg and good solubility and easily formed the thin film when the samples were cast from THF solution. Moreover, the liquid crystalline birefringence did not disappear until the samples were

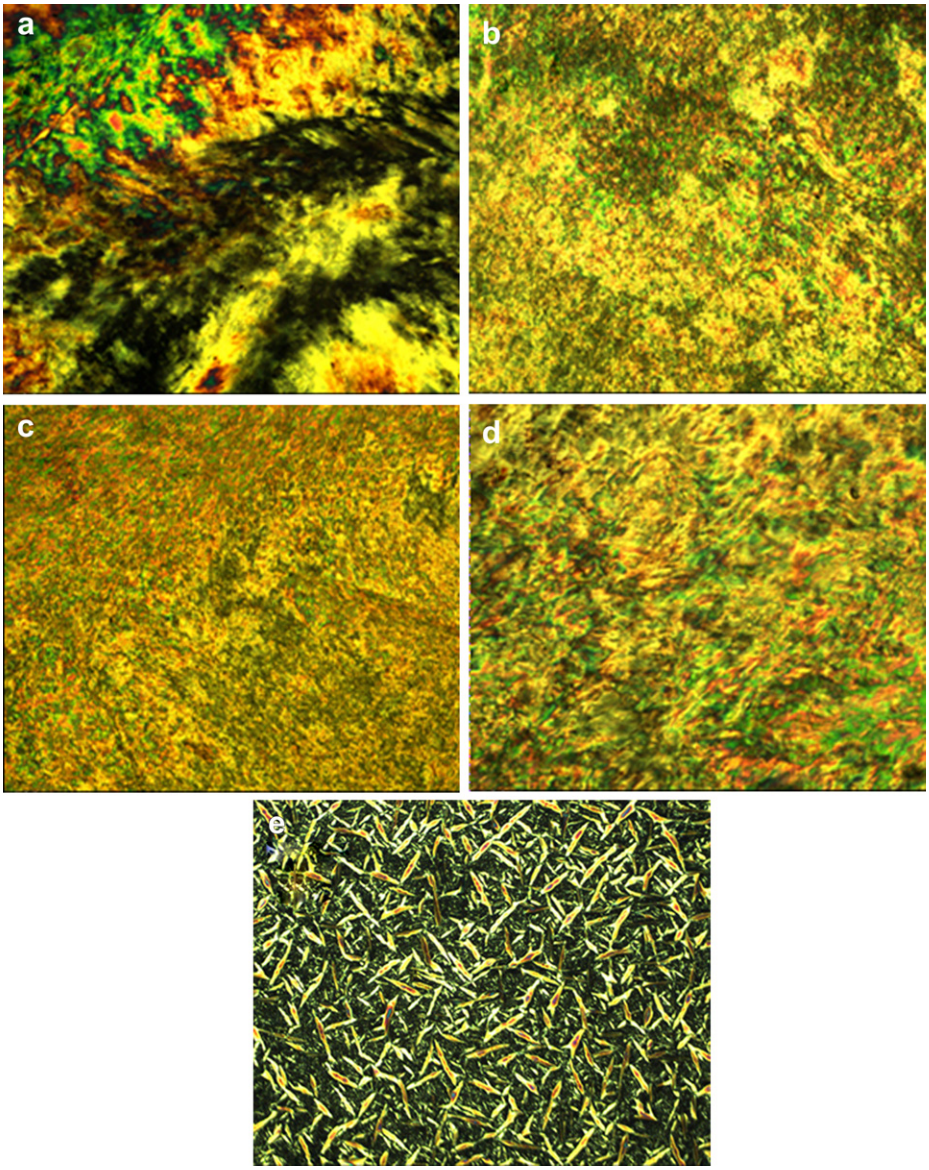

Fig. 6. Representative POM images of the texture of P-C8 (a), P-C10 (b), P-C12 (c), P-C14 (d) and P-C18 (e) at 150 °C (Magnification: ×200).

decomposed. When cooled to room temperature from 310 °C, the birefringence of the sample remained the same, implying that the ordered structure kept unchanged upon cooling.

In order to study the phase transitions and the phase structures of P-Cm's at different temperatures, 1D WAXD experiments were performed. About 60 mg of the polymer was added into an aluminum foil substrate. In order to be consistent with the DSC results, the samples were heated to 250 °C, and then slowly cooled to the room temperature. The temperature was not higher than 280 °C during the experiments for all samples to avoid thermal degradation. Fig. 7(a) and (b) illustrates the temperature-variable 1D WAXD patterns of P—C8 from 50 to 250 °C and from 250 to 50 °C in the 2θ region from 2.5° to 30°. At low angle, one narrow reflection peak was observed at 50 °C, which was lower than the Tg of the homopolymer (226 °C), indicating the ordered structures on the nanometer scale formed ($2\theta = 1.98°$, which a d-spacing value of 4.47 nm). The intensity of the halo basically kept the same with the temperature elevated, i.e., 250 °C, which was higher than the Tg of the polymer, only the peak shifted slightly to high 2θ value due to the thermal expansion. In the wide-angle region of $2\theta > 10°$, only an amorphous halo around 20° could be recognized. This reflected that no long range ordered structure formed via molecular packing was detected over the entire temperature region studied. From the 1D WXRD results, the homopolymers formed the stable LC phase. Moreover, we presume that the structure of the LC phase is layer S_A phase based on two points. On the one hand, calculated length of the mesogenic units is 4.58 nm when the alkane takes trans conformation (the length of side chain will increase 0.25 nm with increasing per two methylene). In our experiment data, the maximum d-spacing value is 4.47 nm, which is close to the calculated length (4.58 nm). On the other hand, the side chains have the strong interactions between biphenyl. Meantime, the long flexible alkoxy tails are immiscible with the rigid core and need larger space in packing. So the polymers form layer $S_{A.}$ In addition, no noticeable change could be observed during the second heating and cooling processes in 1D-WAXD experiments, implying that there was no isotropic phase for P-C8 in the temperature region from 50 to 250 °C.

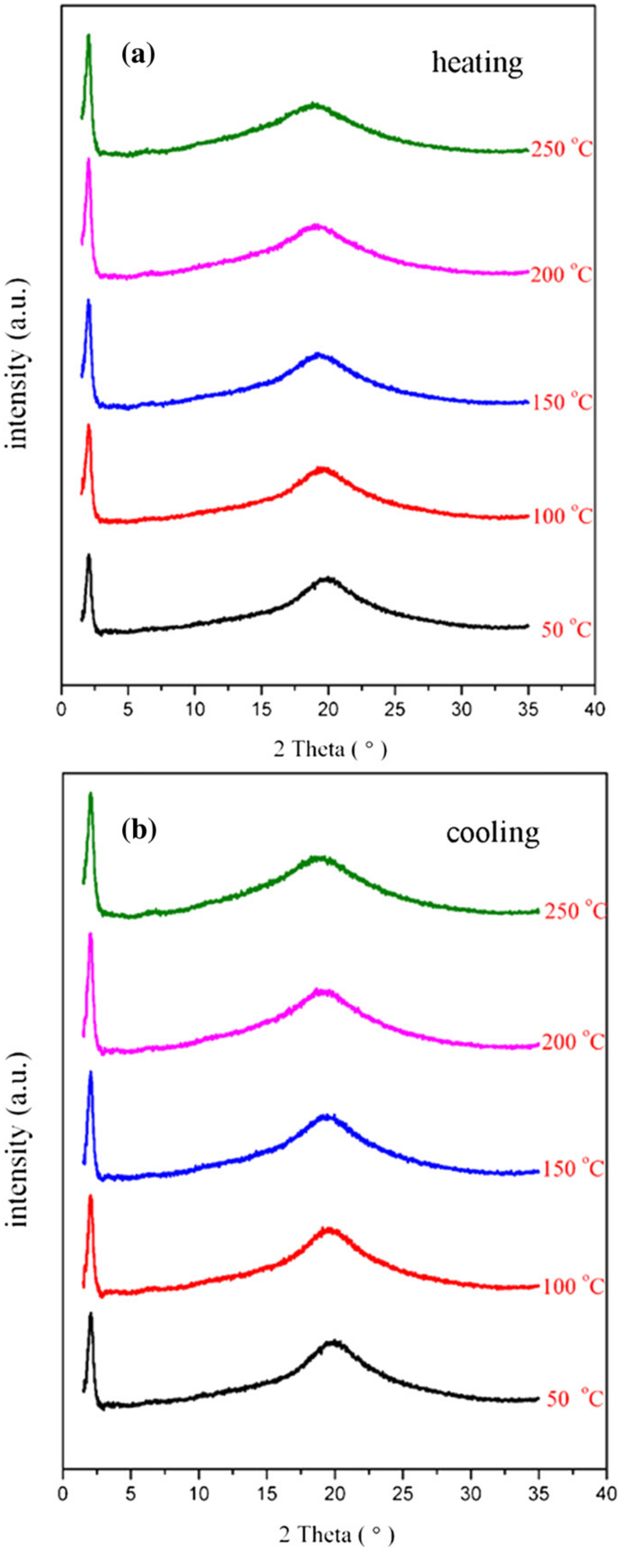

Fig. 7. 1D WAXD patterns of the P-C8 during (a) the second heating process and (b) the second cooling process.

Table 3
The 2θ, d-spacing values and calculated length of the mesogenic units.

Sample	2θ(°)[a]	d-spacing (nm)[a]	Calculated length of the mesogenic units (nm)[b]
P-C8	1.98	4.47	4.58
P-C10	1.85	4.78	5.04
P-C12	1.80	4.94	5.54
P-C14	1.72	5.16	6.04
P-C18	1.59	5.56	7.04

[a] Obtained from the two-dimensional WAXD experiments.

[b] Assuming the n-alkoxy tails in the side chains have an all-trans conformation.

All other P-Cm ($m = 10$, 12, 14 and 18) showed similar results in 1D WAXD experiments, indicating that all polymers formed the S_A phase (see Fig. S2 in Supporting information). The d-spacing values are shown in Table 3. Compared to the theoretic value, the scale of d-spacing is smaller when $m \geq 12$. For this point, it may be caused by two facts. One was, it was impossibility to take trans conformation for all alkane, leading to the increase of theoretical memsogen unit length. Another one, the polymers formed layer structure where the alkyl tails were interdigitated with each other, further leading to the decrease of the d-spacing. Meantime, the 2θ of the polymer is close to the minimum detection value, leading no other peaks to be found. In order to further elucidate the phase structure, we performed 1D SAXS experiment. The samples were heated to 250 °C, then, slowly cooled to the room temperature. Fig. 8 shows the temperature-variable SAXS profiles of P–C18 from 25 to 200 °C. As can be seen from it, a first-order sharp peak is centered at $q^* = 1.04\ \text{nm}^{-1}$ and a higher-order diffraction peak appear at $2q^* = 2.11\ \text{nm}^{-1}$. The ratio of the scattering vectors of the two peaks q^*:$2q^*$ was 1:2, indicating a smectic structure with a periodicity of 5.60 nm ($d100 = 2\pi/q^*$) for P-C18, which is consistent with the 1D WAXD results (5.56 nm). Similar results were obtained from different samples in P-Cm ($m = 8$, 10, 12, and 14).

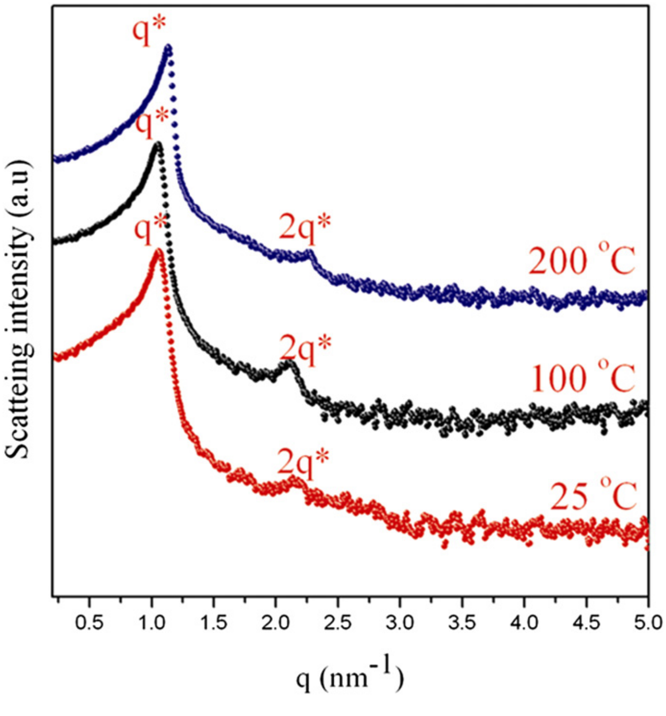

Fig. 8. SAXS profiles of P-C18 recorded during the second heating process with intensity in log scale.

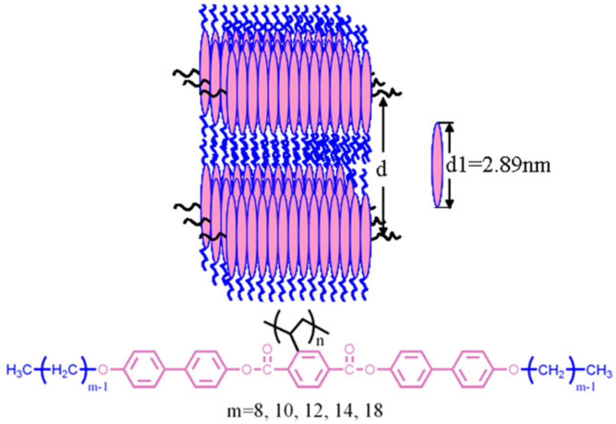

Fig. 9. Schematic drawing of the polymers.

Based on DSC, POM, XRD and SAXS experiments results, we have demonstrated that the polymers of P-Cm ($m = 8$, 10, 12, 14 and 18) presented the stable smectic A (S_A) phase. Compared with the phase behaviors of P-OCm, the P-Cm with the same length alkyl tail has higher Tg and only formed the stable S_A phase with the larger smectic layer period. As the side chain is laterally jacketed to the polymer backbone through a short linkage, the parallel packing of the mesogenic groups makes the polymer molecules somewhat ribbon-like and form ordered S_A phase. So we presume that the schematic drawing of the polymers with rigid symmetry mesogenic core is shown in Fig. 9.

4. Conclusions

We have successfully synthesized a series of vinyl monomers M-Cm ($m = 8$, 10, 12, 14 and 18) containing different length of alkoxy terminal chains. Upon using conventional radical polymerization, we further obtained the corresponding mesogen-jacketed liquid crystalline polymers. The chemical structures of the monomers and polymers were confirmed by various characterization techniques. Their phase structures and transitions of the polymers were investigated with DSC, temperature-variable FT-IR spectroscopy, POM, 1D WAXD and SAXS. The experimental results revealed that MJLCPs formed smectic phase, which indicated that the lateral substitution of long rigid mesogens strongly reduced the ability of forming columnar polymers, although the monomers exhibited the nematic phase.

Acknowledgment

This research was financially supported by the Innovation Platform Open Foundation of University of Hunan Province (10k067), the National Nature Science Foundation of China (51073131, 21174117, 21104062). The authors thank Prof. Chen Er-Qiang and Chen Xiao-Fang of Peking University for their help with 1D WAXD and SAXS experiments measurements.

Appendix A. Supplementary data

Supplementary data related to this article can be found at http://dx.doi.org/10.1016/j.polymer.2013.01.048.

References

[1] Gao LC, Shen ZH, Fan XH, Zhou QF. Polym Chem 2012;3:1947–57.
[2] Chen XF, Shen ZH, Wan XH, Fan XH, Chen EQ, Ma YG, et al. Chem Soc Rev 2010;39:3072–101.
[3] Tamai N, Miyasaka H. Chem Rev 2000;100:1875–90.
[4] Natansohn A, Rochon P. Chem Rev 2002;102:4139–76.
[5] Yu Y, Nakano M, Ikeda T. Nature 2003;425:145.
[6] Percec V, Glodde M, Hudson SD, Duan H. Nature 2002;419:384–7.
[7] Li ZP, Garza P, Baer E, Ellison CJ. Polymer 2012;53:3245–52.
[8] Tokita M, Okuda S, Yoshihara S, Takahashi C, Kang S, Sakajiri K, et al. Polymer 2012;53:5596–9.
[9] Tokita M, Kato K, Ishige R, Okuda S, Kawauchi S, Okoshi K, et al. Polymer 2011;52:5830–5.
[10] Jo TS, Nedeltchev AK, Biswas B, Han H, Bhowmik PK. Polymer 2012;53:1063–71.
[11] Meng FB, Zhang XD, He XZ, Lu H, Ma Y, Han HL, et al. Polymer 2011;52:5075–84.
[12] Kawatsuki N, Shoji H, Yamaguchi K, Kondo M, Tsubaki K. Polymer 2011;52:5788–94.
[13] Finkelmann H, Wendorff HJ. Structure of nematic side chain polymers. In: Blumstein A, editor. Polymeric liquid crystals. New York: Plenum; 1985. p. 295.
[14] Zhou QF, Li HM, Feng XD. Macromolecules 1987;20:233–4.
[15] Zhou QF, Zhu XL, Wen ZQ. Macromolecules 1989;22:491–3.
[16] Zhu ZG, Zhi JG, Liu AH, Cui JX, Tang H, Qiao WQ, et al. J Polym Sci Part A: Polym Chem 2007;45:830–47.
[17] Ye C, Zhang HL, Huang Y, Chen EQ, Lu YL, Shen DY, et al. Macromolecules 2004;37:7188–96.
[18] Zhao YF, Fan XH, Wan XH, Chen XF, Yi Y, Wang LS, et al. Macromolecules 2006;39:948–56.
[19] Xu YD, Yang Q, Shen ZH, Chen XF, Fan XH, Zhou QF. Macromolecules 2009;42:2542–50.
[20] Wang XZ, Zhang HL, Chen EQ, Wang XY, Zhou QF. J Polym Sci Part A: Polym Chem 2005;43:3232–44.
[21] Guan Y, Chen XF, Shen ZH, Wan XH, Zhou QF. Polymer 2009;50:936–44.
[22] Chen XF, Tenneti KK, Li CY, Bai YW, Zhou R, Wan XH, et al. Macromolecules 2006;39:517–27.
[23] Xie HL, Hu TH, Zhang XF, Zhang HL, Chen EQ, Zhou QF. J Polym Sci Part A: Polym Chem 2008;46:7310–20.
[24] Zhang LY, Shen ZH, Fan XH, Zhou QF. J Polym Sci Part A: Polym Chem 2011;49:3207–17.
[25] Zhang D, Liu YX, Wan XH, Zhou QF. Macromolecules 1999;32:5183–5.
[26] Gopalan P, Andruzzi L, Li X, Ober CK. Macromol Chem Phys 2002;203:1573–83.
[27] Chen S, Zhang LY, Gao LC, Chen XF, Fan XH, Shen ZH, et al. J Polym Sci Part A: Polym Chem 2009;47:505–14.
[28] Chai CP, Zhu XQ, Wang P, Ren MQ, Chen XF, Xu YD, et al. Macromolecules 2007;40:9361–70.
[29] Cheng YH, Chen WP, Shen ZH, Fan XH, Zhu MF, Zhou QF. Macromolecules 2011;44:1429–37.
[30] Cheng YH, Chen WP, Zheng C, Qu W, Fan XH, Zhu MF, et al. Macromolecules 2011;44:3973–80.
[31] Chen S, Jie CK, Xie HL, Zhang HL. J Polym Sci Part A: Polym Chem 2012;50:3923–35.
[32] Zhou SR, Zhao Y, Cai YL, Wang DJ, Han CC, Xu DF. Polymer 2004;45:6261–8.